



# Optimal operation of soft open points in medium voltage electrical distribution networks with distributed generation <sup>☆</sup>



Chao Long, Jianzhong Wu <sup>\*</sup>, Lee Thomas, Nick Jenkins

*Institute of Energy, School of Engineering, Cardiff University, Cardiff CF24 3AA, UK*

## HIGHLIGHTS

- A sensitivity method was developed to visualize an SOP operating region in a graphical manner.
- Time series of SOP set-points were provided considering various load and generation conditions.
- A framework was developed to quantify the SOP operational benefit with different objectives.
- This framework is able to facilitate the network operators to select SOP control schemes.

## ARTICLE INFO

### Article history:

Received 1 August 2016  
Received in revised form 29 September 2016  
Accepted 14 October 2016  
Available online 21 October 2016

### Keywords:

Distributed generation  
Jacobian matrix  
Optimization  
Power electronic  
Soft open point

## ABSTRACT

A soft open point (SOP) is a power electronic device, usually using back-to-back voltage source converters (VSCs), installed at a previously normally open point of a distribution network. Due to its flexible and accurate control of power flows, an SOP is versatile, and increasingly being considered to mitigate voltage and thermal constraints in medium voltage (MV) networks with high penetrations of distributed generation (DG). A Jacobian matrix - based sensitivity method was used to define the operating region of an SOP when the grids/feeders at the two terminals of the SOP have various load and generation conditions, and the SOP operating region was visualized in a graphical manner. The exact operating set-points were determined by adopting a non-linear optimization considering separately different objectives. The methodology was demonstrated on an 11 kV network, considering three optimization objectives with different DG penetrations and different network observabilities. Results showed that the use of an SOP significantly increases the network's DG hosting capacity. The objective for voltage profile improvement increased the headroom of the voltage limits by the largest margin, at the expense of increased energy losses. In contrast the objectives to achieve line utilization balancing and energy loss minimization showed the most improvement in circuit utilization and in limiting energy losses. The work helps electricity network operators to visualize an SOP's operation status, and provides high level decision support, e.g. selecting control schemes and restraining SOP operational boundaries.

© 2016 The Authors. Published by Elsevier Ltd. This is an open access article under the CC BY license (<http://creativecommons.org/licenses/by/4.0/>).

## 1. Introduction

With the ambitions of reducing carbon emissions and enhancing energy security and affordability, the integration of distributed generators (DGs) into electrical power systems is being widely promoted by countries across the globe. Medium voltage (MV) distribution networks, to which DGs are connected directly (e.g., wind

farms) or through the aggregation of installations in low voltage networks (e.g., residential-scale photovoltaic systems), are already facing technical challenges in areas where clusters of DG exist. Voltage excursions and thermal overloading are among the dominant issues that limit the ability of MV networks to host large volumes of DG.

Instead of costly network reinforcement, various devices and control schemes have been investigated to mitigate the impacts of DG on distribution networks [1–10].

Traditionally voltage and reactive power control in distribution networks was achieved by on-load tap changers (OLTCs) and shunt capacitors. In [1,2], in order to increase the penetration of DG in an MV network, OLTCs, and shunt capacitors were coordinated by the time delays of their operation, where shorter time delays were set

<sup>\*</sup> This work has been partly funded by the UK-China NSFC/EPSC OPEN project (EP/K006274/1 and 51261130473), the UK-India DST/EPSC (EP/K036211/1) and the Horizon 2020 project P2P-SmartTest.

<sup>\*</sup> Corresponding author.

E-mail addresses: [chao.long.10@gmail.com](mailto:chao.long.10@gmail.com) (C. Long), [wuj5@cardiff.ac.uk](mailto:wuj5@cardiff.ac.uk) (J. Wu), [thomasl62@cardiff.ac.uk](mailto:thomasl62@cardiff.ac.uk) (L. Thomas), [jenkinsn6@cardiff.ac.uk](mailto:jenkinsn6@cardiff.ac.uk) (N. Jenkins).

## Nomenclature

### Abbreviations

DG	distributed generator
ELM	energy loss minimization
LUB	line utilization balancing
MMC	modular multi-level converter
MV	medium voltage
OLTC	on-load tap changer
PV	photovoltaic
PID	proportional–integral–derivative
SOP	soft open point
SVC	static var compensator
VSC	voltage source converters
VPI	voltage profile improvement

### Symbols

$C_{\delta_i P_{jt}}$	constant coefficient for the sensitivity between voltage angle ( $\delta_i$ ) and the active power injection at node $j$ ( $P_j$ )
$C_{\delta_i Q_{jt}}$	constant coefficient for the sensitivity between voltage angle ( $\delta_i$ ) and the reactive power injection at node $j$ ( $Q_j$ )
$C_{V_i P_{jt}}$	constant coefficient for the sensitivity between voltage magnitude at node $i$ ( $V_i$ ) and the active power injection at node $j$ ( $P_j$ )
$C_{V_i Q_{jt}}$	constant coefficient for the sensitivity between voltage magnitude at node $i$ ( $V_i$ ) and reactive power injection at node $j$ ( $Q_j$ )
$I_k$	actual current at branch $k$
$I_{k \text{ rate}}$	rated current of branch $k$

$J$	Jacobian matrix
$n_l$	total number of branches
$N$	total number of nodes
$P$	active power injection at a node
$P_1$	active power that VSC1 provides to Feeder 1
$P_2$	active power that VSC2 provides to Feeder 2
$P^{\text{loss}}$	power losses of an SOP
$P_T^{\text{loss}}$	power losses of the transformers
$Q$	reactive power injection at a node
$Q_1$	reactive power that VSC1 provides to Feeder 1
$Q_2$	reactive power that VSC2 provides to Feeder 2
$r_k$	resistance of the network branch $k$
$S_1$	maximum apparent power of VSC1
$S_2$	maximum apparent power of VSC2
$T$	time span of the period of interest
$V$	vector of nodal voltage
$ V_i _{\text{SOP}_t}$	voltage magnitude at node $i$ with the SOP
$ V_{\text{nom}} $	target voltage for all nodes of the network for voltage profile improvement
$\delta$	voltage angle
$\Delta\delta_i$	change of voltage angle at node $i$ due to SOP's active and reactive power injection
$\Delta V_i _t$	change of voltage magnitude at node $i$ due to SOP's active and reactive power injection
$\delta_{i\text{SOP}_t}$	voltage angle at node $i$ with the SOP
$Y_{ij}$	admittance between nodes $i$ and $j$

for capacitors at mid-points of feeders, and longer delays for capacitors at the substation and OLTCs. In [3], the coordination between OLTCs and capacitors was achieved by multi-stage control. In the first stage, an optimal schedule for capacitors was determined using a genetic algorithm. In the second stage, the OLTCs were controlled in real time with varying set-points considering the differences between forecast and actual loads. In [4], Static Var Compensator (SVC) devices were also applied to improve voltage profiles in distribution networks with photovoltaic (PV) systems and wind power plants. Moreover, control strategies can also be applied to DG units to mitigate their adverse impacts [5]. In [6], reactive power control of DG was used to compensate the effect of the active power when voltage excursions occur. Similarly, a droop control of DG was proposed in [7] to manage power curtailment and prevent overvoltages in the network.

Network reconfiguration has also been used to mitigate voltage excursions and/or manage power flows in distribution networks with DG [8–10]. Depending on the operating time frame, network reconfiguration can be classified as static or dynamic. Static reconfiguration considers all switches (manually or remotely controlled), and looks for an improved fixed topology at the planning stage (e.g., on a yearly or seasonal basis). Dynamic reconfiguration manages these remotely controlled switches by a centralized control scheme to remove voltage constraints or grid congestion in real time [10].

In this work, a soft open point (SOP) was used to replace the mechanical switch at a previously normally open point of an MV network. An SOP is a power electronic device, usually using back-to-back voltage source converters (VSCs). Such device has also been called “SIPLINK” [11], “DC-link” [12–14], and “SNOP” [15] in the literature.

Compared with network reconfiguration, the use of SOPs has the following advantages of: (1) regulating power flows in a continuous manner; (2) flexible and accurate controllability of active and reactive power. In particular, the control of reactive power at

each terminal is independent; (3) short-circuit currents are not increased when using SOPs, due to the almost instantaneous control of current; and (4) SOPs can be used to connect any group of feeders, e.g., supplied from different substations or at unequal rated voltages [13].

SOP devices have been made commercially available [11], but the control strategies and their impact on power networks have not been thoroughly investigated. The benefits of using SOPs in power networks were analyzed in [13,16,17]. These studies, however, were limited to only a few snapshots, rather than considering SOP operation under different load and generation conditions and over a period of time. A few initiative pilot projects have been trialled using SOPs in MV distribution networks in the UK, such as [18,19], but they are in their early stage of development. As an Ofgem Low Carbon Networks Fund (LCNF) project, Flexible Urban Networks Low Voltage (FUN-LV) (initiated by UK Power Networks Ltd) has explored the use of SOP in LV networks [20]. Dual- or multi-terminal SOPs have been trialled across 36 networks. Different control modes, i.e. transformer equalization, voltage support, power factor support, and unbalance support, were applied to different networks adopting a hysteresis method. They did not consider the sensitivity of these control features, i.e. transformer loading, voltage, power factor, and network unbalance, to the SOP's active and reactive power injection. Moreover, there were no detailed models investigating the different effects of active and reactive power from an SOP on the networks. A VSC interconnected with an AC grid, is a nonlinear coupled double-input double-output control object [21]. In [22] a PID (proportional–integral–derivative) controller was adopted to design the transfer function where the active and reactive power were de-coupled and active power was to manage voltage angle and reactive power was to regulate the magnitude. Therefore, to obtain a model and subsequent design of controllers, a mathematical analysis which simultaneously considers the active and reactive power injection from VSCs is required. On the other hand, the model needs to be general to be

applicable to networks with different topologies. In [23,24], an optimization framework, so-called Intervals of Secure Power Injection method, was developed to maximize admissible sets of power injections for secure network operation under marginal changes in network topology.

In this paper, a Jacobian matrix - based sensitivity method, which considers the correlation of the power injections of the SOP with the nodal voltages and line currents of the network, was used to define the operating region of an SOP when the grids/feeders at the two terminals of the SOP have various load and generation conditions. The exact operating set-points of the SOP were determined by using a non-linear optimization where three objectives, i.e. voltage profile improvement, line utilization balancing and energy loss minimization, were considered. The main contributions include: (1) representing the operating region of an SOP in a graphical manner by using a Jacobian matrix - based sensitivity method; (2) providing time series of set-points for an SOP when the grids/feeders at the two terminals of the SOP have various load and generation conditions; and (3) quantifying benefits and shortcomings of different optimization objectives, which will help Distribution Network Operators (DNOs) to select SOP control schemes.

## 2. Problem formulation

### 2.1. Modelling of Soft Open Point (SOP)

Fig. 1 shows a one line diagram of an MV distribution network with an SOP connected at the remote ends of two feeders. The two VSCs (i.e.VSC1 and VSC2) are connected via a common DC bus.  $P_1$  and  $Q_1$  represent the active and reactive power that VSC1 provides to Feeder 1, and  $P_2$  and  $Q_2$  are the active and reactive power that VSC2 provides to Feeder 2.

In a general case,  $n$  ( $n \geq 2$ ) feeders can be connected through an SOP composed of  $n$  VSCs sharing the same DC bus. The AC terminal of each VSC is normally connected to an AC network via a coupling transformer. An SOP with two- or multi- VSCs introduces additional degrees of flexibility for network operation, and the power flow through the SOP can be adjusted within operating limits.

In this work, an SOP with two VSCs (i.e. two AC terminals) is considered. The power provided by an SOP can be modulated in the four quadrants of the power chart, and each VSC can operate in any region of the four quadrants. Fig. 2 shows an example of an SOP's operating point where two VSCs operate in region I and II, respectively. The two axes in Fig. 2 are for the active and reactive power. Positive values represent the VSC providing power and negative values represent the VSC absorbing power. The circles represent the size (i.e. maximum apparent power,  $S_1, S_2$ ) of the corresponding VSC. The power provided by the VSCs cannot exceed their ratings, as shown in

$$\sqrt{(P_1)^2 + (Q_1)^2} \leq S_1 \quad (1)$$

$$\sqrt{(P_2)^2 + (Q_2)^2} \leq S_2 \quad (2)$$

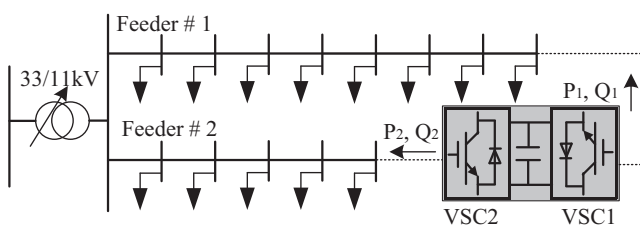


Fig. 1. An MV network with an SOP at the remote ends of two feeders.

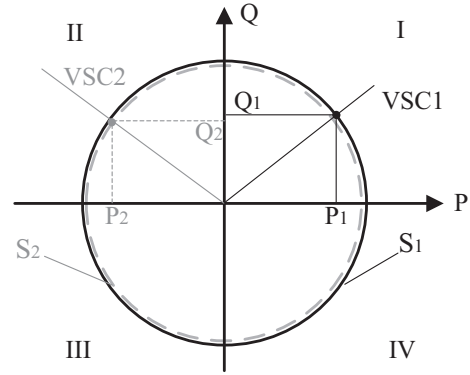


Fig. 2. An example of an SOP's operating point: active and reactive power provided by an SOP with two VSCs having the same rating (for illustration purposes, the circle for VSC2 is smaller than VSC1 in the figure).

With appropriate control, both VSCs produce their individual voltage waveforms with the desired amplitude and phase angle. This provides full (four-quadrant) control of the active and reactive power at both AC terminals. The reactive powers provided, or absorbed, by the two terminals, i.e.  $Q_1, Q_2$ , are independent; whilst the active powers, i.e.  $P_1$  and  $P_2$ , are not independent variables, as the sum of the active powers should be equal to zero, as shown in

$$\sum_{j=1,2} (P_j + P^{loss}) = 0 \quad (3)$$

where  $P^{loss}$  is the power losses of the SOP, including losses in the converters (conduction and switching losses), the DC link capacitor, the filter and the coupling transformers.

With the use of the modular multi-level converter (MMC) technology, the operating loss of a VSC is relatively low, approximately 1% per converter [25]. Therefore, for simplicity, the losses of the SOP are neglected, and Eq. (3) reduces to

$$\sum_{j=1,2} P_j = 0 \quad (4)$$

The SOP adopted is based on the MMC VSC technology at a commercially available size [11]. The SOP is capable of providing the required power within its operational constraint. The detailed control principle of the VSCs can be found in [26].

### 2.2. Jacobian matrix based sensitivity analysis

The sensitivity of voltages and currents in a network to the SOP's active and reactive power injections was analyzed using the Jacobian matrix [27]. For all the PQ buses, the voltage sensitivity to the bus injection of active and reactive power is calculated from

$$\begin{bmatrix} \Delta\delta \\ \Delta|V|/|V| \end{bmatrix} = J^{-1} \begin{bmatrix} \Delta P \\ \Delta Q \end{bmatrix} = \begin{bmatrix} \frac{\partial P}{\partial \delta} & |V| \frac{\partial P}{\partial |V|} \\ \frac{\partial Q}{\partial \delta} & |V| \frac{\partial Q}{\partial |V|} \end{bmatrix}^{-1} \times \begin{bmatrix} \Delta P \\ \Delta Q \end{bmatrix} \quad (5)$$

where  $V$  is the vector of the nodal voltage, and  $\delta$  is the voltage angle;  $P$  and  $Q$  are the injection of active and reactive power at a node;  $J$  is the Jacobian matrix.

The Jacobian matrix changes over time as the network configuration and load and generation conditions vary. For a given time instant,  $t$ , the Jacobian matrix is considered constant, and the corresponding inverse matrix is expressed by

$$J_t^{-1} = \begin{bmatrix} C_{\delta_2 P_{2t}} & \cdots & C_{\delta_2 P_{Nt}} & C_{\delta_2 Q_{2t}} & \cdots & C_{\delta_2 Q_{Nt}} \\ \vdots & \cdots & \vdots & \vdots & \cdots & \vdots \\ C_{\delta_N P_{2t}} & \cdots & C_{\delta_N P_{Nt}} & C_{\delta_N Q_{2t}} & \cdots & C_{\delta_N Q_{Nt}} \\ C_{V_2 P_{2t}} & \cdots & C_{V_2 P_{Nt}} & C_{V_2 Q_{2t}} & \cdots & C_{V_2 Q_{Nt}} \\ \vdots & \cdots & \vdots & \vdots & \cdots & \vdots \\ C_{V_N P_{2t}} & \cdots & C_{V_N P_{Nt}} & C_{V_N Q_{2t}} & \cdots & C_{V_N Q_{Nt}} \end{bmatrix} \quad (6)$$

where  $N$  is the total number of nodes.  $C_{\delta_i P_j t}$  is a constant coefficient for the sensitivity between voltage angle,  $\delta_i$ , and the active power injection at node  $j$ .  $C_{\delta_i Q_j t}$  is a constant coefficient for the sensitivity between  $\delta_i$  and the reactive power injection at node  $j$ .  $C_{V_i P_j t}$  is a constant coefficient for the sensitivity between voltage magnitude at node  $i$ ,  $V_i$  and  $P_j$ .  $C_{V_i Q_j t}$  is a constant coefficient for the sensitivity between  $V_i$  and  $Q_j$ ,  $i = 2, 3, 4, \dots, N$ ,  $j = 2, 3, 4, \dots, N$ . Note that node 1 is a “slack” or “infinite” bus, where the voltage magnitude is specified and phase angle is assumed to be zero. Therefore it is not included in the Jacobian matrix.

At time instant  $t$ , the sensitivity of voltage angle and magnitude at node  $i$  are calculated by

$$\Delta \delta_{it} = \sum_{j=2}^N (C_{\delta_i P_j t} * \Delta P_{jt} + C_{\delta_i Q_j t} * \Delta Q_{jt}) \quad (7)$$

$$\Delta |V_i|_t = |V_i|_t * \sum_{j=2}^N (C_{V_i P_j t} * \Delta P_{jt} + C_{V_i Q_j t} * \Delta Q_{jt}) \quad (i = 2, 3, 4, \dots, N) \quad (8)$$

It is assumed that, at time instant  $t$ , apart from the SOP's active and reactive power injections, the change in active and reactive power at all nodes is zero. Despite the variations in demand and generation, the control of the SOP is able to be made as fast as milliseconds when using the power electronic devices [26]. There might be delays in data measurement and communications which will result in delay of the SOP control and require a sophisticated control algorithm design, but this is out of the scope of this work. The assumption made here allows the impact of the SOP on the network to be analyzed, and more rigorous studies on real-time control of the SOP will be carried out in the future. Hence, the voltage angle and magnitude at node  $i$  are presented as

$$\delta_{i_{SOPt}} = \delta_{it} + \Delta \delta_{it} \quad (9)$$

$$|V_i|_{SOPt} = |V_i|_t + \Delta |V_i|_t \quad (i = 2, 3, 4, \dots, N) \quad (10)$$

where  $\Delta \delta_{it}$  and  $\Delta |V_i|_t$  only consider SOP's active and reactive power injections.

### 2.3. Optimization formulation

Three optimization formulations were considered, each with a different objective. For each optimization formulation, the voltage angle and magnitude at node  $i$  (i.e.  $\delta_{i_{SOPt}}$ ,  $|V_i|_{SOPt}$ ) were calculated by Eqs. (7)–(10), and the active and reactive power provided by the two VSCs were the decision variables.

#### 2.3.1. Voltage Profile Improvement (VPI)

When improving the voltage profile of the network is desired, the objective function is

$$\min \sum_{i=1}^N (|V_i|_{SOPt} - |V_{nom}|)^2 \quad (11)$$

where  $|V_{nom}|$  is a target voltage for all nodes of the network.

This objective function leads to an optimal dispatch of the SOP's active and reactive power values to bring all nodal voltages as close as possible to the target value. The nominal voltage, i.e. 1 p.u., was

taken as the target voltage, because this is considered as a mid-point of the future scenarios, given that the integration of DG results in voltage rise and the electrification of transport and heating leads to low voltages.

#### 2.3.2. Line Utilization Balancing (LUB)

When the line utilization of the network is to be balanced, the objective function is

$$\min \sum_{k=1}^{n_l} \left( \frac{I_k}{I_{k \text{ rate}}} \right)^2 \quad (12)$$

where  $n_l$  is the total number of branches, and  $I_k$  and  $I_{k \text{ rate}}$  are the actual and rated current of branch  $k$ . Assuming that the node numbers of the two terminals of the branch  $k$  are  $i$  and  $j$ , and  $Y_{ij}$  is the admittance between nodes  $i$  and  $j$ , the actual current in the branch  $k$  can be expressed by

$$I_k = Y_{ij} * (|V_i|_{SOP} \angle \delta_{i_{SOP}} - |V_j|_{SOP} \angle \delta_{j_{SOP}}) \quad (13)$$

This objective function leads to an optimal dispatch of the SOP's active and reactive power values to achieve balancing of line utilization.

#### 2.3.3. Energy Loss Minimization (ELM)

When the energy losses of the network are to be minimized, the objective function is

$$\min \sum_{t=0}^T \left( \sum_{k=1}^{n_l} (I_k)^2 * r_k + P_{T \text{ loss}} \right) * t \quad (14)$$

where  $P_{T \text{ loss}}$  is the power losses of the transformers,  $r_k$  is the resistance of the network branch  $k$ , and  $T$  is the time span of the period of interest.

This objective function leads to an optimal dispatch of the SOP's active and reactive power values to achieve the lowest line and transformer energy losses.

#### 2.3.4. Constraints

Together with the constraints shown in (1), (2) and (4), the operation of the network cannot breach the voltage and thermal limits, as shown in

$$V_{min} \leq |V_i|_{SOPt} \leq V_{max} \quad (15)$$

$$|I_k| \leq I_{k \text{ rate}} \quad (16)$$

### 3. Visualization of the SOP operating region

Considering the voltage constraints, the SOP's active and reactive power operating region is visualized in the four quadrants of the power chart. For illustration purposes, the charts for four different scenarios are presented.

- Undervoltage in Feeder 1, undervoltage in Feeder 2 (Fig. 3);
- Undervoltage in Feeder 1, voltage within limit in Feeder 2 (Fig. 4);
- Undervoltage in Feeder 1, overvoltage in Feeder 2 (Fig. 5);
- Overtension in Feeder 1, overvoltage in Feeder 2 (Fig. 6).

“Undervoltage”, “overvoltage”, and “voltage within limit” are used to define the feeder voltage status without considering the SOP's power injection. “Undervoltage” in a feeder means that the feeder is relatively heavily loaded, and undervoltage occurs when there is no power injection from the VSC. “Overvoltage” means that the feeder has more distributed generation, and overvoltage occurs when there is no power injection from the VSC. “Voltage within

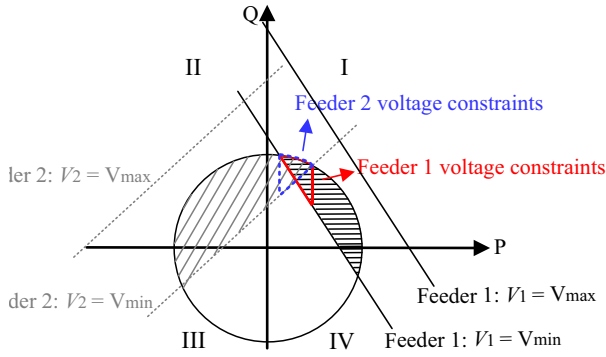


Fig. 3. VSC operating regions with voltage constraints: undervoltage in Feeder 1 and undervoltage in Feeder 2 (VSC2 mirrored in y-axis).

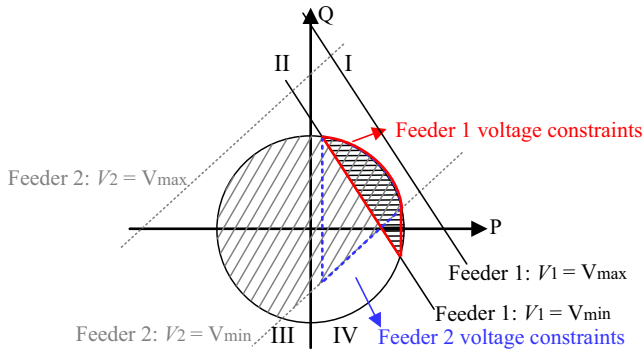


Fig. 4. VSC operating regions with voltage constraints: undervoltage in Feeder 1 and within limit in Feeder 2 (VSC2 mirrored in y-axis).

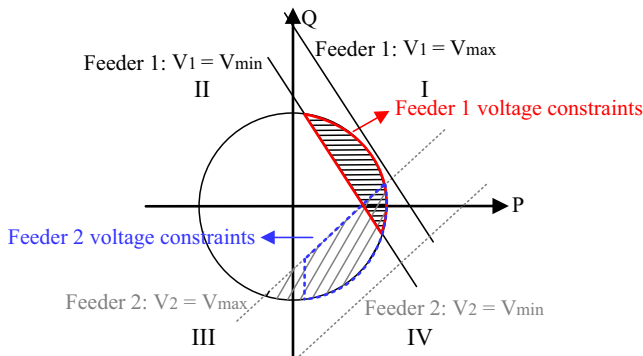


Fig. 5. VSC operating regions with voltage constraints: undervoltage in Feeder 1 and overvoltage in Feeder 2 (VSC2 mirrored in y-axis).

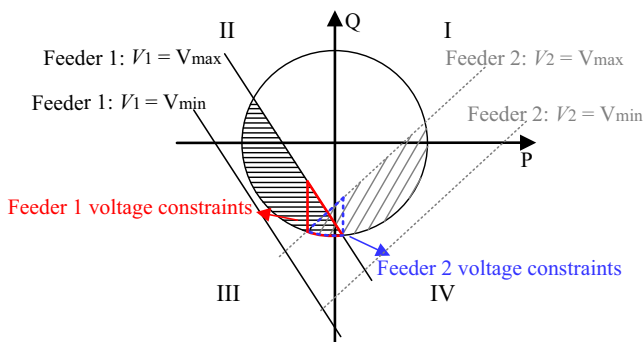


Fig. 6. VSC operating regions with voltage constraints: overvoltage in Feeder 1 and overvoltage in Feeder 2 (VSC2 mirrored in y-axis).

Table 1  
Operating region in a four quadrant chart of an SOP.

		Feeder 1		
		Undervoltage	Voltage within limit	Overvoltage
Feeder 2	Undervoltage	I, II	I, II, III	II, III
	Voltage within limit	I, II, IV	–	II, III, IV
	Overvoltage	I, IV	I, III, IV	III, IV

limit” means that the voltages in the feeder is within the limits when there is no power injection from the VSC.

Fig. 3 shows two overlaid circles representing the active and reactive power limits for the two VSCs of the SOP, assuming the two VSCs are the same size. The circle for VSC2 (connected to Feeder 2) was mirrored in the y-axis so that the allowable operating region can be visualized. This is done because the active power of the two SOP terminals must be symmetric (see Eq. (4)). As a consequence, for any operating point in Fig. 3, Eq. (4) is met.

In Fig. 3, the two solid (and dashed) lines represent the lower and upper voltage limits of Feeder 1 (and Feeder 2). These lines are constant voltage loci, i.e. the active and reactive power operating points on each line bring the voltage to the same value. The boundary of the voltage limits was obtained from Eq. (15), and the  $|V_{i|SOP}|$  in Eq. (15) was calculated from Eqs. (10) and (8). The linear relation of the nodal voltages to the active and reactive power from the SOP shown in Eq. (8) resulted in linear boundaries when considering the voltage limits. Therefore, to keep voltages in Feeder 1 (and Feeder 2) within the limits, the SOP’s active and reactive power values must be within the two solid (and dashed) lines. The common active and reactive power operating points on the circle, where VSC1 and VSC2 share the same active power values (i.e. on a vertical line), are the operating regions for each VSC (i.e. the voltage constraint for each feeder). Therefore, the ultimate voltage constraints for the two feeders are shown in the red and blue blocks.

Similarly, the voltage constraints for scenarios (b)–(d) are presented in Figs. 4–6. These figures present the active and reactive power regions where the SOP should operate under various scenarios.

In a general case, the SOP’s active and reactive power operating region varies depending on the actual voltages and the sensitivity of the voltages to the active and reactive power injections of the SOP (i.e. slope of the constant voltage loci) of the two feeders. “Undervoltage”, “overvoltage”, and “voltage within limit” were in a way to reflect a feeder’s load and generation conditions. The graphical method provides a general idea of active and reactive power regions at which an SOP operates when the two feeders are under various load and generation scenarios, see Table 1. A qualitative analysis with a graphical visualization not only helps network operators to understand an SOP’s operating status, but also provides high level operational decision support, such as choosing control schemes, and restraining operational boundaries.

## 4. Case study

### 4.1. MV distribution network model

An example distribution network obtained from [28] was used with some modifications. As shown in Fig. 7, the 11 kV network consists of four radial feeders (three-phase underground cables) with different lengths (each segment is 1 km) and load types. The rated capacity of the 33/11 kV transformer is 20 MVA. An SOP is connected at the remote ends of Feeder 2 and Feeder 3, with a rated capacity of 3 MVA for each VSC. Various DGs are installed at different locations to represent the expected load/generation distribution between feeders. Table 2 shows a summary of the load

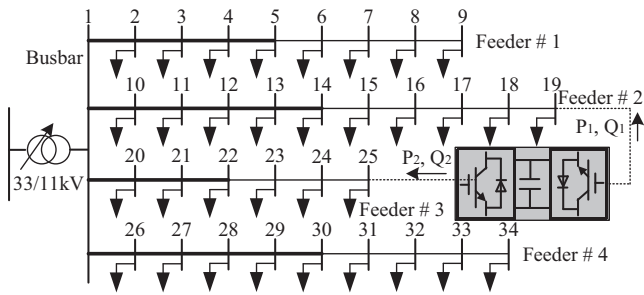


**Fig. 7.** One line diagram of a radial MV network (the cable diameters of the first half of the feeders, i.e. closer to the substation, are bigger than the second half, therefore they are shown in thicker lines).

and generation data. The impedance of the first half of the feeder (close to the substation) is  $0.164 + j0.08 \Omega/\text{km}$ , and the rated current is 335 A per phase, and the second half is  $0.320 + j0.087 \Omega/\text{km}$ , with a rated current of 230 A per phase.

Fig. 8 shows the profiles for residential, commercial and industrial loads for two days (a weekend day and a weekday), with power factors of 0.98, 0.95, and 0.90. Fig. 9 shows the generation profiles for wind and PV systems for the two days under study, and all wind and PV generations are considered to operate at unity power factor. These load data was obtained from [29] and wind and PV generation data was obtained from [28], and these data are presented in the Appendix of this paper. These load and generation profiles are all normalized to their own peak values, and the corresponding peak load of a feeder and the peak of a DG unit are shown in Table 2.

Power flow calculations of the network were carried out in MATLAB using the Newton-Raphson method, and the tolerance of iteration was considered as 0.001 per unit. Jacobian matrix was obtained when the power flow solution reached convergence. Then the non-linear programming optimization with non-linear constraints was also carried out in MATLAB, where an Interior-Point algorithm and Hessian matrix were used to find the optimal solutions. The power flow calculations and optimizations were run at each time step, i.e. every 30 min, for the proposed three objective functions. The relevant computation experiments were performed on a desktop machine, Intel (R) Core (TM) i7-4790 CPU @ 3.6 GHz, 16 GB RAM and MATLAB version R2014a, and the optimization process for each time step is approximately 450 milliseconds.

4.2. DG penetration level

DG penetration level is defined as the total of the rating of each individual DG in the network in relation to the 33/11 kV transformer rated capacity, as shown in

$$\text{Penetration Level} = \frac{\text{Sum of all DG ratings}}{33/11 \text{ kV transformer rating}} \quad (17)$$

Various penetration scenarios were considered by scaling up/down the rating of each DG. For instance, the DG rating (MW) values shown in Table 2 represent a DG penetration level of 60%.

**Table 2**  
Load and DG data.

Feeder #.	Load		Distributed generation		
	Type	Total peak (MVA)	Type	Locations	Ratings (MW)
1	Com.	3	Wind	5, 9	2, 0.5
2	Res.	2.5	PV	11, 14, 17	1, 2, 2.5
3	Ind.	3	Wind	22, 25	0.5, 2.5
4	Res.	2.5	PV, wind	30, 33	0.5, 0.5

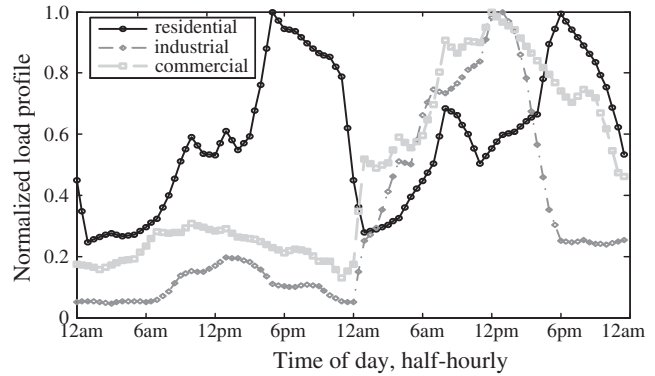


**Fig. 8.** Load profiles of the network (a weekend day and a weekday, data obtained from [29]).

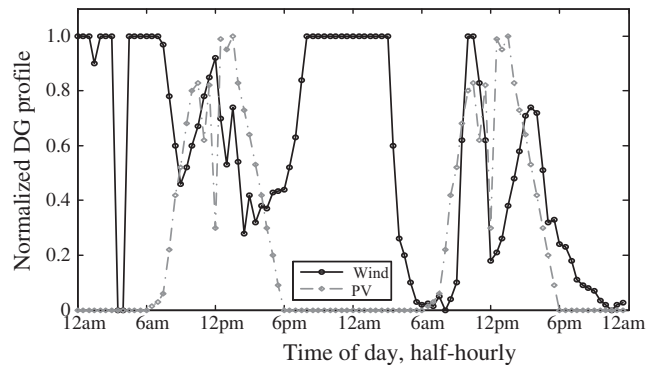


**Fig. 9.** Wind and PV profiles of the network (data obtained from [28]).

With these DG rating (MW) values halved, the penetration level is 30%. With 1.5 times of these DG rating (MW) values, the penetration level is 90%.

4.3. Two-day performance with a 90% DG penetration – full observability of the network

Fig. 10 shows the performance of the network with the SOP and a 90% DG penetration.  $\pm 3\%$  of nominal was considered as the voltage limit [16,30]. Fig. 10(a) presents the active and reactive power consumption of the network. Part (b) of the figure is the voltage profiles at the busbar and remote ends of the four feeders without an SOP. Part (c) and part (d) are the dispatched active and reactive power values of the SOP and voltage profiles when optimizing the voltage profile using the VPI objective. The dispatched active and reactive power values and the resultant voltage profiles when using the line balance LUB and energy loss ELM objectives are shown in part (e) and (f), and part (g) and (h).

Note that, without an SOP, overvoltages occurred in Feeder 2 and Feeder 3. These overvoltages did not occur when using an SOP, irrespective of the objective function used. When using the VPI objective, the voltage profiles were better (i.e. closer to the 1 pu target value) than when using the LUB or ELM objective. In

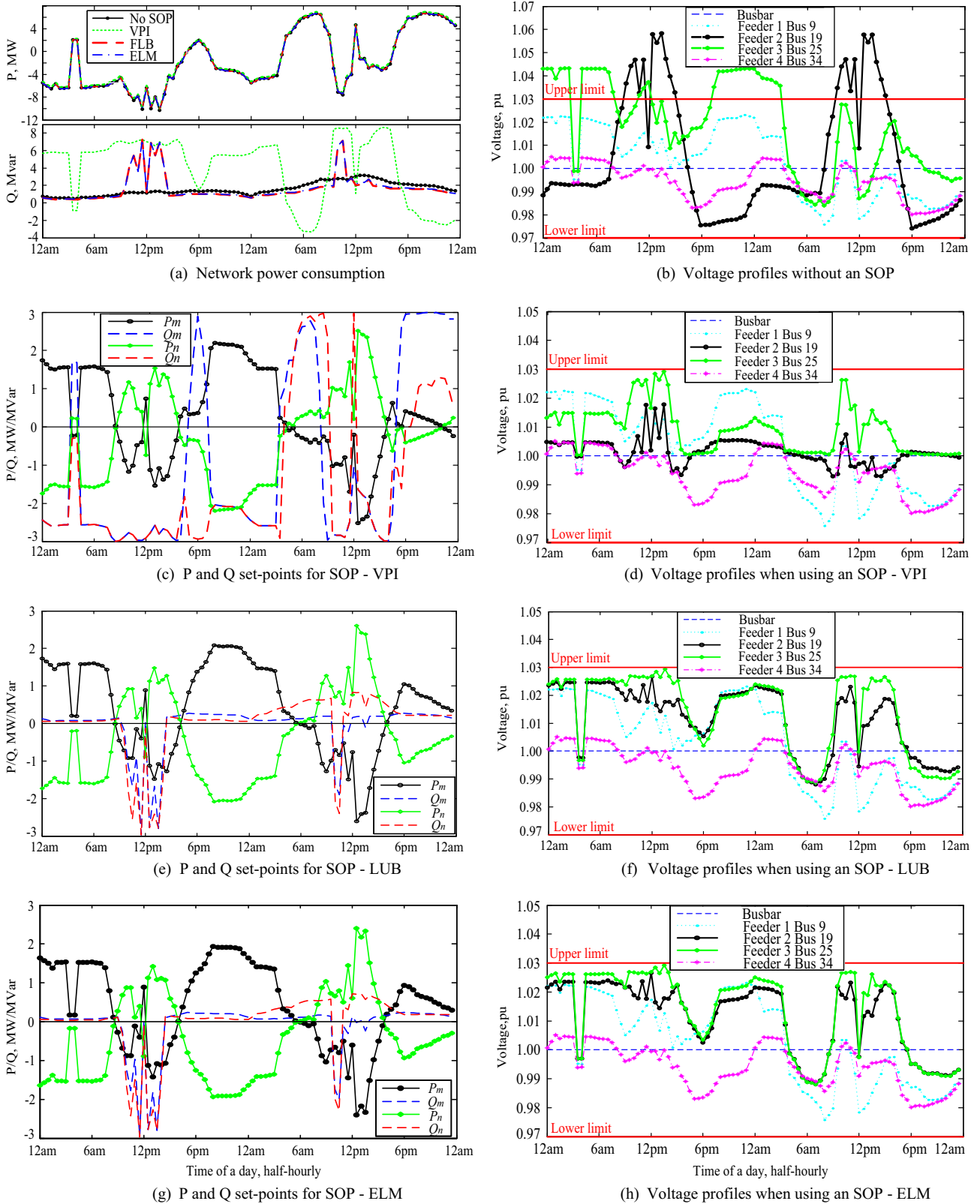


Fig. 10. Two-day performance of SOP for a 90% DG penetration.

terms of dispatched active and reactive power values from the SOP, the active values were similar when adopting the three objective functions. However, more reactive power from SOP was dispatched when using the VPI objective than when using the LUB or ELM objective.

The dispatched active and reactive power values (i.e. set-points) of the SOP are shown in the four quadrant power chart in Fig. 11. As shown, more operating points were close to, or on, the edge of the circle using the VPI objective than using the LUB or the ELM objective, and this also illustrates more reactive power from

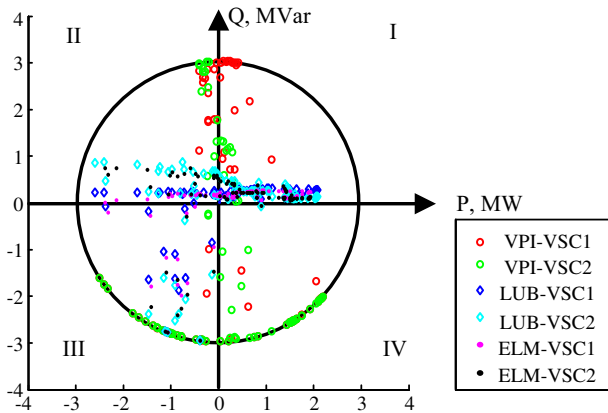


Fig. 11. P and Q set-points of the SOP for different optimization objectives and a 90% DG penetration.

SOP was dispatched using the VPI objective. The objectives to achieve line balancing LUB and energy loss minimization ELM mainly relied on real power exchange.

4.4. Overall performance – full observability of the network

The network performance was examined by investigating the maximum and minimum voltages, the maximum line utilization and the energy losses of the network with DG penetration from 0 to 90% (10% per step), and they are presented in Figs. 12–14.

Without using an SOP, overvoltages were present from 60% DG penetration, see Fig. 12. When using an SOP and disregarding the objective function used, the network reached 90% DG penetration without violating the voltage limits. The maximum voltages were kept lower when optimizing the voltage profile using the VPI objective than when using the line balance LUB or energy loss ELM objective, along all DG penetrations.

As shown in Fig. 13, for DG penetrations from 10% to 60%, the maximum line utilization was always larger when adopting the VPI objective than the case without an SOP. This was because the increased reactive power injection from the SOP resulted in an increase in the currents of some circuits. However, a slight decrease was shown when the penetration was more than 70%. This was because with higher penetrations of DG, the VSCs of the SOP began to consume reactive power reducing currents of some parts of the network. When using the LUB or the ELM objective, the maximum line utilization was always smaller than the case without an SOP, for all DG penetrations.

In Fig. 14, it is shown that, by using the VPI objective, the total energy losses were approximately twice those without an SOP. Considering only the loads (i.e. 0% DG penetration), the total

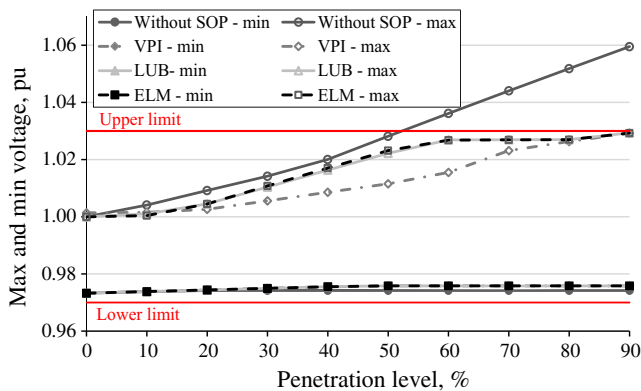


Fig. 12. Maximum and minimum voltage – full network observability.

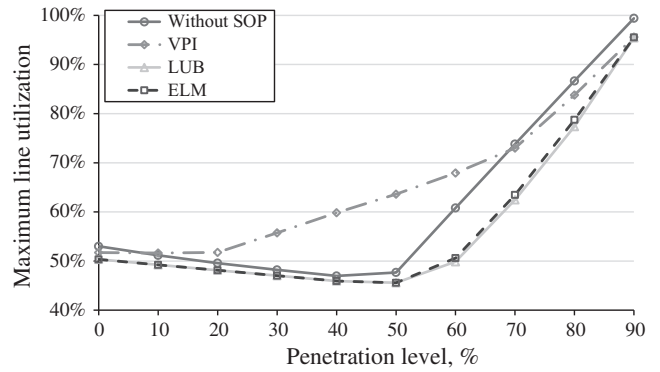


Fig. 13. Maximum loading (line utilization) – full network observability.

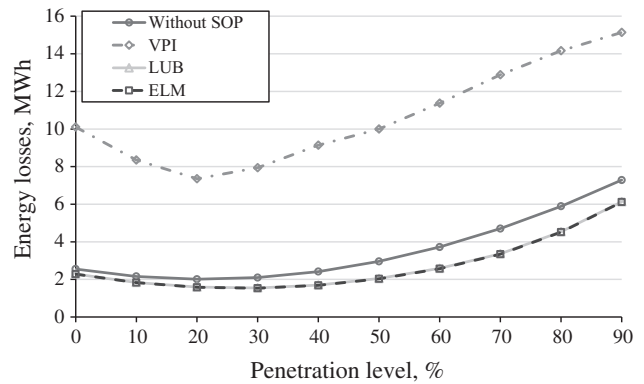


Fig. 14. Total energy losses for the two days – full network observability.

energy losses for the two days were 2.55 MWh, which corresponds to approximately 1% of the total energy consumption. With a 90% DG penetration, and without an SOP, the total energy losses were 7.28 MWh (i.e. ~2.9% of the total energy consumption). Also, due to the increased dispatch of reactive power, adopting the VPI objective resulted in a significant increase in losses, where the total energy losses were 15.1 MWh (i.e. ~5.9% of the total energy consumption). In contrast, a reduction of energy losses was shown throughout all penetration levels when adopting LUB or ELM as the objective. For a 90% DG penetration, the energy losses when using the LUB were 6.13 MWh, and using the ELM the energy losses were 6.12 MWh, and both showed a slight reduction compared to the case without an SOP.

4.5. Overall performance – limited & no observability of the network

In reality, the control system will not have full network observability. A case in which loads were 20% smaller than the optimization input data was considered, assuming all DGs were correctly measured. The reduction rate for each load was randomly selected from a range of 10–30%, and the overall load reduction was 20%. This was a simple assumption made here to represent a global measurement error, when a network has limited measurements. The overall performance of the network is shown in Table 3. In this table, voltages above the limit are marked in red. It is seen that, when using the LUB and ELM objectives, overvoltages were present from 70% DG penetration; whilst, when using the VPI objective, the voltages were within the limits until the DG penetration reached 90%. For the network without an SOP, as the DG penetration increased, voltage excursions were encountered before thermal overloading. Therefore, the method optimizing voltage profiles, VPI, performed better than the line utilization balancing or loss

**Table 3**

Overall performance of the network with limited network observation (Numbers in bold denote that the relevant voltage magnitude exceeds the voltage limits).

Penetration level, %	Without an SOP				Voltage profile improvement				Line utilization balancing				Energy loss minimization			
	Voltage, pu		Max line use, %	Losses, MWh	Voltage, pu		Max line use, %	Losses, MWh	Voltage, pu		Max line use, %	Losses, MWh	Voltage, pu		Max line use, %	Losses, MWh
	Min	Max			Min	Max			Min	Max			Min	Max		
0	0.973	1.000	53.0	2.55	0.978	1.000	49.9	9.4	0.978	1.000	41.5	1.48	0.978	1.000	41.5	1.46
10	0.974	1.004	51.2	2.16	0.979	1.004	48.9	7.7	0.979	1.003	39.9	1.14	0.979	1.002	39.9	1.12
20	0.974	1.009	49.6	2.01	0.979	1.007	49.2	6.8	0.979	1.007	39.5	1.01	0.979	1.007	39.5	0.98
30	0.974	1.014	48.2	2.10	0.979	1.007	56.8	7.5	0.979	1.012	39.5	1.08	0.979	1.013	39.5	1.05
40	0.974	1.020	47.0	2.42	0.979	1.009	61.2	8.7	0.979	1.017	39.5	1.34	0.979	1.019	39.5	1.31
50	0.974	1.028	47.7	2.96	0.979	1.012	65.4	9.7	0.979	1.023	42.3	1.79	0.979	1.025	45.2	1.76
60	0.974	<b>1.036</b>	60.8	3.72	0.979	1.016	70.0	11.1	0.979	1.029	53.7	2.44	0.979	1.029	54.4	2.41
70	0.974	<b>1.044</b>	73.8	4.70	0.979	1.024	75.4	12.7	0.979	<b>1.032</b>	65.9	3.31	0.979	<b>1.032</b>	66.9	3.28
80	0.974	<b>1.052</b>	86.7	5.89	0.979	1.028	86.5	14.0	0.979	<b>1.032</b>	80.5	4.57	0.979	<b>1.032</b>	81.8	4.54
90	0.974	<b>1.059</b>	99.4	7.28	0.979	<b>1.031</b>	98.5	15.1	0.979	<b>1.032</b>	98.3	6.26	0.979	<b>1.032</b>	98.4	6.23

minimization method (e.g. LUB or ELM), in terms of mitigating the network voltage and thermal constraints.

At minimal network observability, only the voltages at the SOP terminals are known by the SOP control system. In this case, the optimization formation with the voltage improvement VPI as the objective was used, and Eq. (11) only considered the voltages at the two terminals rather than all the nodes. It is found that, by using an SOP, the network's DG hosting capacity was increased from 50% to 80%.

## 5. Discussion

For the visualization of an SOP's operating region, the voltage limit boundaries (shown in Figs. 3–6) represent the most sensitive or the worst node voltage in a feeder. This node is most likely to be the remote end for a one-line MV feeder and might be another node for a grid/feeder with different topologies. However, Jacobian matrix based sensitivity method is able to provide the relation of voltage at any point of a network with the power injection of an SOP, irrespective of the network topology, therefore the methodology is applicable to different topologies, e.g. feeders with many laterals/branches.

An SOP with a given rating and location was considered. This research can be a framework for higher level studies, including finding the optimal number and size of SOPs with different network topologies and configurations. When a network is equipped with multiple SOPs, Eqs. (9) and (10) should include all the terminals of all SOPs. When the two feeders, to which an SOP is connected, are supplied by different substations, one Jacobian matrix is calculated for each substation, and two sets of Equations similar to (9) and (10) are created in order to include both terminals of the SOP.

Balanced three-phase load and generation were considered. Through adequate control of VSCs, the SOP is able to provide three-phase unbalanced power injections. The method used in this research to quantify the benefit of using an SOP could be applied to a three-phase unbalanced system.

Harmonics brought by VSCs and losses of VSCs, and their impact on the performance of the control schemes were out of the scope of this paper.

In this work, a data set of 30-min granularity with different load and generation conditions was taken. This is because this work is mainly for planning purposes, to provide distribution network operators with high level decision support, e.g. selecting control schemes and restraining SOP operation boundaries. However, given that the optimization calculation for each run took approximately 450 ms, the optimization is able to be run in real time, and the methodology is able to be used for real-time operation purposes.

This work did not consider active control devices, such as battery storage, OLTC, and capacitor banks. The control time frame

of these active control devices is normally minutes or hours. Although some electronic interfaced battery storage is able to change control settings on a millisecond timeframe, due to the battery life time concern, battery banks normally operate in a steady state time frame. In the contrast, SOPs are not constrained by mechanical wear or life time concern therefore are able to change operating points more frequently. On the other hand, this work focuses on the performances of SOP control schemes, and provides decision supports of selecting control schemes. Hence, these active control devices were not considered. Future work can be undertaken investigating the real-time operation of SOP with battery storage systems, OLTC, and capacitor banks.

## 6. Conclusions

A non-linear programming optimization, to set the real and reactive power operating set-points for an SOP on an 11 kV network, was developed. Through a Jacobian matrix based sensitivity analysis, the SOP's operating region was defined within its voltage-limit bounds, and visualized in a graphical manner for different load and generation conditions at the grids or feeders at the two terminals of the SOP. The exact operating point was determined using three optimization objectives: voltage profile improvement, line utilization balancing and energy loss minimization.

Results showed that the use of an SOP significantly increases the network's DG hosting capacity. The control scheme using the objective for voltage profile improvement increased the headroom of the voltage limits by the largest margin. This control scheme dispatched increased reactive power, and, hence, was at the expense of increased energy losses.

The control schemes using the objectives to achieve line utilization balance and energy losses minimization showed the most improvement in circuit utilization and in limiting energy losses, mainly relying on the real power exchange between feeders.

This work does not make a suggestion on which optimization objective is better than others, but presents the performance of each and leaving the selecting options to network operators based on their needs. Defining a unifying cost function is difficult, because the cost of breaching voltage and thermal limits, and cost of energy losses may vary from network to network. According to a network's characteristics, network operators are able to devise the control scheme using one or multi-objective functions. The proposed methodology provides a potential framework/solution for electricity network operators, allowing them to choose appropriate control schemes more effectively. This selection requires the network operators to attribute value to the increase in hosting capacity, mitigation in voltage issues, the reduction in the maximum line utilization and the reduction in energy losses.

## Appendix A

See [Table A1](#).

**Table A1**  
Normalized load and generation data (all normalized to their own peak).

Time	Day 1 (a weekend day)					Day 2 (a weekday)				
	Load			DG		Load			DG	
	Residential	Industrial	Commercial	Wind	PV	Residential	Industrial	Commercial	Wind	PV
00:00	0.449	0.050	0.175	1.000	0.000	0.449	0.050	0.175	1.000	0.000
00:30	0.347	0.052	0.172	1.000	0.000	0.363	0.150	0.347	1.000	0.000
01:00	0.246	0.053	0.169	1.000	0.000	0.278	0.251	0.519	1.000	0.000
01:30	0.255	0.052	0.164	0.900	0.000	0.283	0.272	0.504	1.000	0.000
02:00	0.263	0.051	0.158	1.000	0.000	0.289	0.294	0.490	1.000	0.000
02:30	0.270	0.048	0.165	1.000	0.000	0.297	0.353	0.499	1.000	0.000
03:00	0.276	0.046	0.172	1.000	0.000	0.304	0.411	0.507	1.000	0.000
03:30	0.272	0.050	0.179	0.000	0.000	0.315	0.462	0.549	0.600	0.000
04:00	0.267	0.054	0.186	0.000	0.000	0.326	0.512	0.590	0.260	0.000
04:30	0.269	0.053	0.189	1.000	0.000	0.361	0.506	0.573	0.200	0.000
05:00	0.271	0.053	0.192	1.000	0.000	0.396	0.501	0.556	0.100	0.000
05:30	0.284	0.052	0.214	1.000	0.000	0.422	0.581	0.576	0.030	0.000
06:00	0.297	0.050	0.235	1.000	0.000	0.448	0.662	0.596	0.020	0.000
06:30	0.310	0.054	0.258	1.000	0.015	0.475	0.704	0.647	0.025	0.015
07:00	0.323	0.057	0.281	1.000	0.030	0.503	0.746	0.697	0.015	0.030
07:30	0.361	0.071	0.279	0.970	0.060	0.594	0.739	0.802	0.050	0.060
08:00	0.399	0.085	0.277	0.780	0.220	0.685	0.733	0.907	0.000	0.220
08:30	0.455	0.112	0.278	0.600	0.420	0.674	0.749	0.886	0.040	0.420
09:00	0.511	0.138	0.279	0.460	0.520	0.662	0.765	0.865	0.100	0.520
09:30	0.551	0.145	0.293	0.520	0.680	0.631	0.787	0.885	0.620	0.680
10:00	0.591	0.151	0.307	0.600	0.800	0.600	0.810	0.905	1.000	0.800
10:30	0.563	0.150	0.301	0.670	0.830	0.552	0.824	0.902	1.000	0.830
11:00	0.536	0.149	0.295	0.780	0.620	0.503	0.838	0.899	0.830	0.620
11:30	0.534	0.159	0.289	0.850	0.820	0.528	0.910	0.950	0.620	0.820
12:00	0.532	0.170	0.283	0.920	0.300	0.554	0.981	1.000	0.180	0.300
12:30	0.571	0.183	0.287	0.700	0.990	0.576	0.991	0.983	0.210	0.990
13:00	0.610	0.196	0.291	0.530	0.950	0.598	1.000	0.966	0.260	0.950
13:30	0.580	0.195	0.277	0.740	1.000	0.603	0.968	0.955	0.380	1.000
14:00	0.549	0.194	0.263	0.540	0.830	0.608	0.936	0.943	0.480	0.830
14:30	0.570	0.188	0.261	0.280	0.730	0.625	0.860	0.915	0.580	0.730
15:00	0.592	0.182	0.259	0.420	0.640	0.643	0.784	0.887	0.710	0.640
15:30	0.676	0.170	0.255	0.320	0.530	0.654	0.675	0.864	0.740	0.530
16:00	0.760	0.158	0.250	0.380	0.420	0.665	0.566	0.841	0.720	0.420
16:30	0.880	0.134	0.240	0.370	0.300	0.780	0.459	0.818	0.510	0.300
17:00	1.000	0.110	0.230	0.430	0.200	0.895	0.353	0.795	0.320	0.200
17:30	0.972	0.106	0.221	0.435	0.090	0.945	0.302	0.768	0.330	0.090
18:00	0.944	0.102	0.212	0.440	0.000	0.995	0.251	0.741	0.240	0.000
18:30	0.941	0.101	0.218	0.520	0.000	0.968	0.249	0.722	0.230	0.000
19:00	0.938	0.100	0.225	0.630	0.000	0.941	0.247	0.703	0.180	0.000
19:30	0.918	0.104	0.221	0.840	0.000	0.916	0.250	0.725	0.110	0.000
20:00	0.898	0.108	0.217	1.000	0.000	0.891	0.253	0.746	0.090	0.000
20:30	0.881	0.106	0.201	1.000	0.000	0.863	0.247	0.733	0.080	0.000
21:00	0.865	0.103	0.184	1.000	0.000	0.835	0.241	0.720	0.070	0.000
21:30	0.858	0.088	0.184	1.000	0.000	0.794	0.241	0.669	0.035	0.000
22:00	0.852	0.072	0.184	1.000	0.000	0.753	0.240	0.618	0.020	0.000
22:30	0.820	0.062	0.157	1.000	0.000	0.687	0.245	0.545	0.000	0.000
23:00	0.789	0.053	0.131	1.000	0.000	0.622	0.250	0.473	0.020	0.000
23:30	0.619	0.051	0.153	1.000	0.000	0.534	0.253	0.461	0.028	0.000
24:00	0.449	0.050	0.175	1.000	0.000	0.445	0.256	0.448	0.040	0.000

## References

- [1] Viawan FA, Karlsson D. Voltage and reactive power control in systems with synchronous machine-based distributed generation. *IEEE Trans Power Del* 2008;23(2):1079–87.
- [2] Viawan FA, Sannino A, Daalder J. Voltage control with on-load tap changers in medium voltage feeders in presence of distributed generation. *Electr Power Syst Res* 2007;77(10):1314–22.
- [3] Park JY, Nam SR, Park JK. Control of a ULTC considering the dispatch schedule of capacitors in a distribution system. *IEEE Trans Power Syst* 2007;22(2):755–61.
- [4] Savić A, Đurišić Z. Optimal sizing and location of SVC devices for improvement of voltage profile in distribution network with dispersed photovoltaic and wind power plants. *Appl Energy* 2014;134:114–24.
- [5] Kabir MN, Mishra Y, Ledwich G, Xu Z, Bansal RC. Improving voltage profile of residential distribution systems using rooftop PVs and Battery Energy Storage systems. *Appl Energy* 2014;134:290–300.
- [6] Carvalho PMS, Correia PF, Ferreira LAFM. Distributed reactive power generation control for voltage rise mitigation in distribution networks. *IEEE Trans Power Syst* 2008;23(2):766–72.
- [7] Tonkoski R, Lopes LAC, El-Fouly THM. Coordinated active power curtailment of grid connected PV inverters for overvoltage prevention. *IEEE Trans Sustain Energy* 2011;2(2):139–47.
- [8] Dorostkar-Ghamsari MR, Fotuhi-Firuzabad M, Lehtonen M, Safdarian A. Value of distribution network reconfiguration in presence of renewable energy resources. *IEEE Trans Power Syst* 2016;31(3):1879–88.
- [9] Bernardon DP, Mello APC, Pfitscher LL, Canha LN, Abaide AR, Ferreira AAB. Real-time reconfiguration of distribution network with distributed generation. *Elect Power Syst Res* 2014;107:59–67.
- [10] Capitanescu F, Ochoa LF, Margossian H, Hatzigaryriou ND. Assessing the potential of network reconfiguration to improve distributed generation hosting capacity in active distribution systems. *IEEE Trans Power Syst* 2015;30(1):346–56.

- [11] Flottesmesch J, Rother M. Optimized energy exchange in primary distribution networks with DC links. Proceedings of Electric Utility DRPT 2004, Hong Kong, China, vol. 1. p. 108–16.
- [12] Tang CY, Chen YF, Chen YM, Chang YR. DC-link voltage control strategy for three-phase back-to-back active power conditioners. *IEEE Trans Indust Electron* 2015;62(10):6306–16.
- [13] Romero-Ramos E, Gómez-Expósito A, Marano-Marcolini A, Maza-Ortega JM, Martínez-Ramos JL. Assessing the loadability of active distribution networks in the presence of DC controllable links. *IET Gener Transm Distrib* 2011;5(11):1105–13.
- [14] Maza-Ortega JM, Gómez-Expósito A, Barragán-Villarejo M, Romero-Ramos E, Marano-Marcolini A. Voltage source converter-based topologies to further integrate renewable energy sources in distribution systems. *IET Renew Power Gener* 2012;6(6):435–45.
- [15] Cao W, Wu J, Jenkins N. Feeder load balancing in MV distribution networks using soft normally-open points. In: 2014 IEEE PES ISGT-Europe, Istanbul, Turkey. p. 1–6.
- [16] Bloemink JM, Green TC. Benefits of distribution-level power electronics for supporting distributed generation growth. *IEEE Trans Power Del* 2013;28(2):911–9.
- [17] Cao W, Wu J, Jenkins N, Wang C, Green T. Benefits analysis of Soft Open Points for electrical distribution network operation. *Appl Energy* 2016;165:36–47.
- [18] Western Power Distribution. Low Carbon Networks Fund submission from Western Power Distribution – Network Equilibrium Available <<https://www.ofgem.gov.uk/publications-and-updates/low-carbon-networks-fund-submission-western-power-distribution-%E2%80%93-network-equilibrium>>; 2016.
- [19] SP Energy Networks. Electricity NIC submission: SP Energy Networks – ANGLE-DC Available <<https://www.ofgem.gov.uk/publications-and-updates/electricity-nic-submission-sp-energy-networks-angle-dc>>; 2016.
- [20] UK Power Networks. Flexible Urban Networks – Low Voltage (FUN LV) Available <<http://innovation.ukpowernetworks.co.uk/innovation/en/Projects/tier-2-projects/Flexible-Urban-Networks-Low-Voltage/>>; 2016.
- [21] Kalantar M, Mousavi SM. Dynamic behavior of a stand-alone hybrid power generation system of wind turbine, microturbine, solar array and battery storage. *Appl Energy* 2010;87:3051–64.
- [22] Trujillo CL, Velasco D, Guarnizo JG, Díaz N. Design and implementation of a VSC for interconnection with power grids, using the method of identification the system through state space for the calculation of controllers. *Appl Energy* 2011;88:3169–75.
- [23] Georgiev D et al. Computing intervals of secure power injection. *IFAC Proc* 2014;47(3):2253–9.
- [24] Vor P et al. Modular algorithms for computing Intervals of Secure Power Injection. In: 2016 IEEE international energy conference (ENERGYCON).
- [25] Jones PS, Davidson CC. Calculation of power losses for MMC-based VSC HVDC stations. In: 2013 15th European Conference on Power Electronics and Applications (EPE), Lille. p. 1–10.
- [26] Cao W, Wu J, Jenkins N, Wang C, Green T. Operating principle of Soft Open Points for electrical distribution network operation. *Appl Energy* 2016;164:245–57.
- [27] Mutale J, Strbac G, Curcic C, Jenkins N. Allocation of losses in distribution systems with embedded generation. *IEE Proc Gener Transm Distrib* 2000;147(1):7–14.
- [28] Farag HEZ, El-Saadany EF. A novel cooperative protocol for distributed voltage control in active distribution systems. *IEEE Trans Power Syst* 2013;28(2):1645–56.
- [29] DTI Centre for Distributed Generation and Sustainable Electrical Energy. United Kingdom Generic Distribution System Phase One, March 2006. Available <<http://www.sedg.ac.uk/ukgds.htm>>.
- [30] Masters CL. Voltage rise: the big issue when connecting embedded generation to long 11 kV overhead lines. *Power Eng J* 2002;16(1):5–12.